ORIGINAL ARTICLE

WILEY

Three-dimensional kinematics of the canine carpal bones imaged with computed tomography after ex vivo axial limb loading and palmar ligament transection

Jack D. Neville-Towle BVSc[1] (iD) | **Christopher J. Tan BVSc, DECVS[1,2]** |
William C. H. Parr PhD[2] | **William R. Walsh PhD[2]** |
Kenneth A. Johnson MVSc, PhD, DACVS, DECVS[1]

[1] Sydney School of Veterinary Science, Faculty of Science, The University of Sydney, Sydney, Australia

[2] Surgical and Orthopaedic Research Laboratories, Prince of Wales Clinical School, Prince of Wales Hospital, University of New South Wales, Sydney, Australia

Correspondence
Jack Neville-Towle, Evelyn Williams Building B10, Sydney School of Veterinary Science, Faculty of Science, The University of Sydney, Sydney, Australia.
Email: jacknevilletowle@gmail.com

The copyright line for this article was changed on 5 August 2019 after original online publication

Abstract

Objective: To describe normal antebrachiocarpal joint kinematic motion during axial loading and to describe the effect of palmar radiocarpal ligament (PRL) and palmar ulnocarpal ligament (PUL) transection on this motion.

Sample population: Ten forelimbs from 5 adult greyhound cadavers.

Methods: Limbs were placed in a custom jig and computed tomography images of limbs were obtained in neutral and extended positions. The translation and rotation of the intermedioradiocarpal bone (RCB), ulnar carpal bone, and accessory carpal bone were described relative to the radius through rigid body motion analysis. Kinematic and load analysis was repeated after sequential transection of the PRL and the PUL.

Results: Sagittal plane extension with a lesser component of valgus motion was found in all evaluated carpal bones. RCB supination was also detected during extension. Compared with the normal intact limb, transection of either or both the PRL and the PUL did not influence mean translation or rotation data or limb load. However, the transection of the PRL and the PUL increased the variance in rotation data compared with intact limb.

Conclusion: This study describes normal antebrachiocarpal kinematics as a foundation for determining carpal functional units. During axial loading, the PRL and the PUL may function to guide consistent motion in extension and flexion as well as pronation and supination.

Clinical significance: Three-dimensional carpal kinematic analyses may improve our understanding of carpal injury and facilitate the development of novel treatments techniques.

1 | INTRODUCTION

The canine carpus comprises proximal, middle, distal, and intercarpal articulations, which, collectively, function as a

ginglymus.[1] Kinematic studies have described the overall motion of the canine carpus using external markers.[2] For example, maximal carpal extension angle during weight bearing has recently been found to exceed 60°.[3] In man, computed tomography (CT) has been used to segment bone surfaces and describe the translation and rotation of bones of the wrist by using a Cartesian coordinate system.[4] These noninvasive techniques have been found to measure

accurately the motion of the wrist, including maximum range of motion during flexion and extension of the wrist.[5] Currently, the kinematics of individual carpal bones has not been described in dogs.

Although the antebrachiocarpal joint contributes most to flexion and extension of the canine carpus, the role and importance of the ligamentous structures at this articulation have been reported infrequently.[1,6] The palmar radiocarpal ligament (PRL) and the palmar ulnocarpal ligament (PUL), in combination with the collateral ligaments, have been found to limit extension of the antebrachiocarpal joint under a defined weight of 2 kg in a cadaveric model.[7] Another observational study in dogs reported that transection of both of the PRL and PUL resulted in palpable dorsal and palmar instability of the manus in flexion and extension and mild hyperextension of the antebrachiocarpal joint.[8] The carpus functions as a "biological spring," able to store "external work."[9,10] However, the contributions of the carpal structures involved in this biological spring, particularly those acting on the antebrachiocarpal joint, vary among reports and remain unclear. This inconsistency warrants investigation to determine the roles of the PRL and the PUL in guiding carpal bone motion under axial loading.

The objective of this study was to describe normal antebrachiocarpal joint kinematics during axial loading and to describe the effect of PRL and PUL transection on this motion. Our first hypothesis was that normal canine antebrachiocarpal kinematics of the intermedioradial carpal bone (RCB), ulnar carpal bone (UCB), or accessory carpal bone (ACB) following gross carpal extension would be limited to sagittal plane extension. Our second hypothesis was that transection of the PRL or the PUL would not significantly affect RCB, UCB, and ACB motion or limb load compared with the normal findings without ligament transection.

2 | MATERIALS AND METHODS

2.1 | Preparation of limbs

Ten forelimbs were obtained from 5 mature, female greyhound cadavers that had been euthanized for reasons unrelated to this study. The cadavers were used in accordance with the University of Sydney's animal ethics regulations. The forelimbs from each cadaver were harvested distal to the humeral diaphysis. The limbs were immediately frozen at −20°C and later thawed within 8 hours of use prior to testing. The origins of the antebrachial musculature, including the digital and carpal flexor and extensor muscles, were preserved. The periarticular soft tissue structures of the elbow were also preserved. The skin proximal to the midmetacarpal region was removed. All limbs were confirmed to be free from evidence of skeletal disease distal to and including the elbow according to review of CT images. A random number

generator was used to assign the left limbs to either group A or group B. The contralateral right limb of each cadaver was assigned to the alternate group.

A 6-mm threaded bolt was placed transversely through the caudoproximal region of the humeral condyle after predrilling of both medial and lateral cortices with a 5-mm drill bit with the limb prepositioned in the jig to maintain accurate distal limb positioning during the latter stages of testing. The humeral bolt was passed through a bracket in a custom-fabricated loading jig. After it had been secured to the bracket, the metacarpal pad was positioned in a marked central location on the baseplate of the jig (Figure 1). The jig permitted rotation of the proximal bracket to allow accurate gross sagittal alignment to be achieved in the transverse plane. Pressure-sensitive film (Tekscan, Boston, Massachusetts) was placed under the digital and metacarpal pads such that the load applied to the carpus could be recorded immediately prior to the acquisition of each CT scan. Each of the carpi used in this study were preconditioned 10 times by increasing load from a neutral (12° carpal extension) position to the extended (60° carpal extension) position and then returning to the neutral position with the scissor-jack in the loading jig. The position of the bolt permitted the radius and ulna to be loaded by the humerus without additional excessive elbow flexion, and a sagitally divided fiberglass cast was used to standardize the carpal extension angle during preconditioning and all CT scans.

2.2 | CT acquisition and load measurement

All limbs were CT scanned (120 kV, 200 mA, slice thickness 1 mm, collimation 16 × 0.75; Y-Sharp filter; Philips, Amsterdam, The Netherlands; 16-slice Brilliance CT; Philips) in neutral and extended carpal positions (Figure 1). CT data were stored in standard Digital Imaging and Communications in Medicine (DICOM) format. The loads applied to the limbs in neutral and extended positions were recorded and reported as mean (±SD) for each position and transection condition. A multiplanar reconstruction of each CT image allowed measurements of the sagittal carpal extension angle. The landmarks for this measurement were the center of the proximal radial articular surface, the center of the distal radial articular surface, and the center of the distal articular surface of metacarpal bone III.

2.3 | Ligament transections

All limbs were unloaded from the jig prior to each arthroscopic ligament transection phase and maintained proximally by the humeral bolt. Two 3-mm ports were created in the antebrachiocarpal joint capsule of each limb, medial and lateral to the extensor carpi radialis tendon.[8] A 2.5-mm, 30° fore-oblique arthroscope was used through the dorsomedial
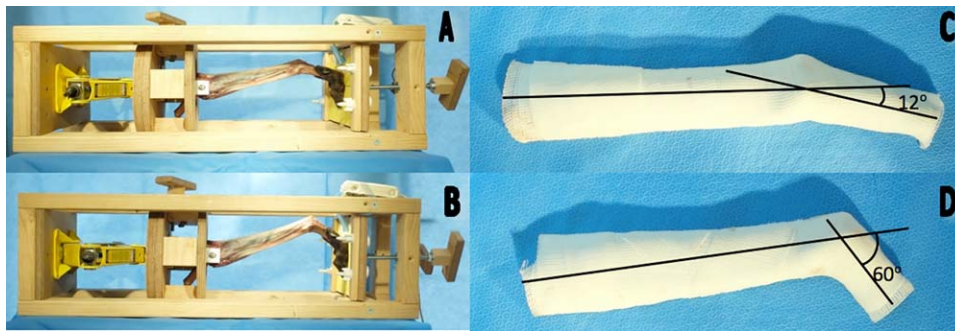
FIGURE 1 **A,B**, Custom-fabricated loading jig with the limb in neutral and extended carpal positions, respectively. **C,D**, Fiberglass cast material was placed over the limbs in neutral and extended positions, respectively. The resultant cast was divided in the sagittal plane and used to check limb angle for the corresponding position of each subsequent limb

port to inspect the antebrachiocarpal joint. An arthroscopic probe was used to identify the PRL and the PUL. Paired limbs were divided into 2 groups (A or B).

Limbs assigned to group A underwent transection of the PRL arthroscopically with a "hook" knife. The limbs were rescanned in the neutral and extended positions, and load was again recorded. The PUL was then arthroscopically transected with either a hook or push knife with the same technique such that both ligaments (PRPU) in these carpi were transected. CT was repeated in neutral and extended positions, and loads were recorded.

The limbs assigned to group B underwent arthroscopic transection of the PUL. CT was repeated in neutral and extended positions, and loads were recorded.
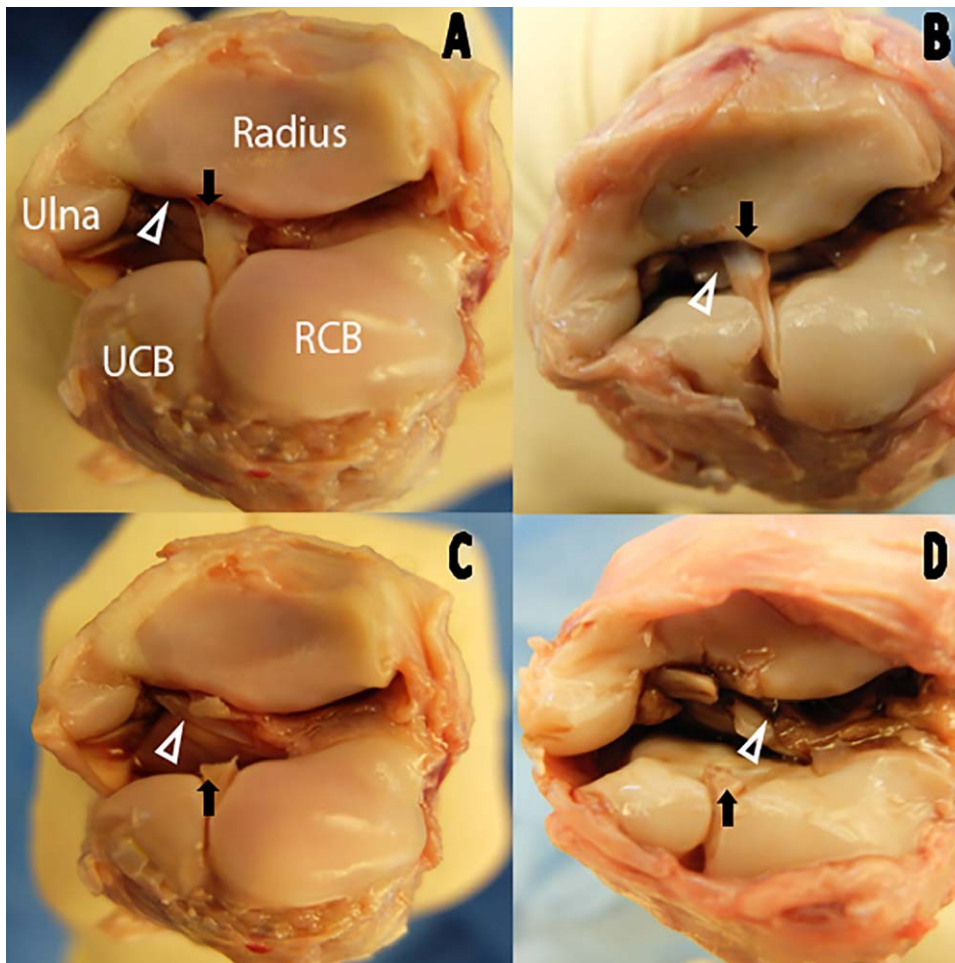
FIGURE 2 Representative gross dissected dorsal views of the transected palmar radiocarpal ligament (black arrow), and palmar ulnocarpal ligament (white arrowhead). **A**, Intact palmar radiocarpal ligament and palmar ulnocarpal ligament. **B**, Transected palmar ulnocarpal ligament. **C**, Transected palmar radiocarpal ligament. **D**, Transection of both palmar ligaments. RCB, intermedioradiocarpal bone; UCB, ulnar carpal bone

After CT acquisition of all limbs, the antebrachiocarpal joint of each limb was dissected to confirm correct and complete ligament transection (Figure 2). Limbs were excluded if either ligament transection was incomplete.

2.4 | CT analyses

All CT DICOM images were imported to medical image processing software (MIMICS version 17.0; Materialise, Leuven, Belgium). An accelerated segmentation tool (CT bone segmentation tool), which, combined the functionality of thresholding, seeded region growing, editing, and 3-dimensional (3D) calculation was used to semiautomate the segmentation of the radius, RCB, UCB, and ACB. Three-dimensional surface models were created by using a predefined smoothing algorithm (1st order laplacian smoothing: factor 0.5, iterations 4) and exported as stereolithography (STL) files.[11] The segmented and smoothed surface models were exported both as individually segmented and as "joined" (radius, RCB, UCB, and ACB) STL files.

The smoothed surface models of the initial neutral scan radius bone from each limb were exported into medical 3D modeling software (3-Matic 8.0; Materialise), and each radius was aligned to a global coordinate system. The alignment method involved use of the centrum of the distal radial articular surface, the craniolateral aspect of the ulnar notch adjacent to the distal joint surface, and the centrum of the proximal radial articular surface (Figure 3A,B). These 3 coordinates allowed a system of axes to be embedded in the radius, which were then superimposed with a Cartesian global coordinate system such that the origin was positioned at the centrum of the distal radial articular surface.[4] Positive rotation around the x-axis represented supination, positive rotation around the y-axis represented flexion, and positive rotation around the z-axis represented valgus. Translations were reported on the basis of the same axes (Figure 3A).

Three-dimensional mesh software was used to superimpose the aligned radius surface model of the first neutral scan with each of the subsequent surface models of the radius, RCB, UCB, and ACB from the same limb.[12] Superimposition was achieved through a 2-step process: (1) a rough initial manual alignment and (2) a subsequent iterative closest point alignment of the unaligned radii with the initially aligned radii.[13] This process aligns the radius and all of the joined carpal bone surface models from each CT to the global coordinate system. Separate, individually segmented RCB, UCB, and ACB models were then sequentially superimposed on the aligned neutral and extended models of the same bone to generate a positional matrix for each bone and condition.

After the STL files of the segmented RCB, UCB, and ACB of each position and transection condition were obtained, mathematical software (Mathematica version 10;
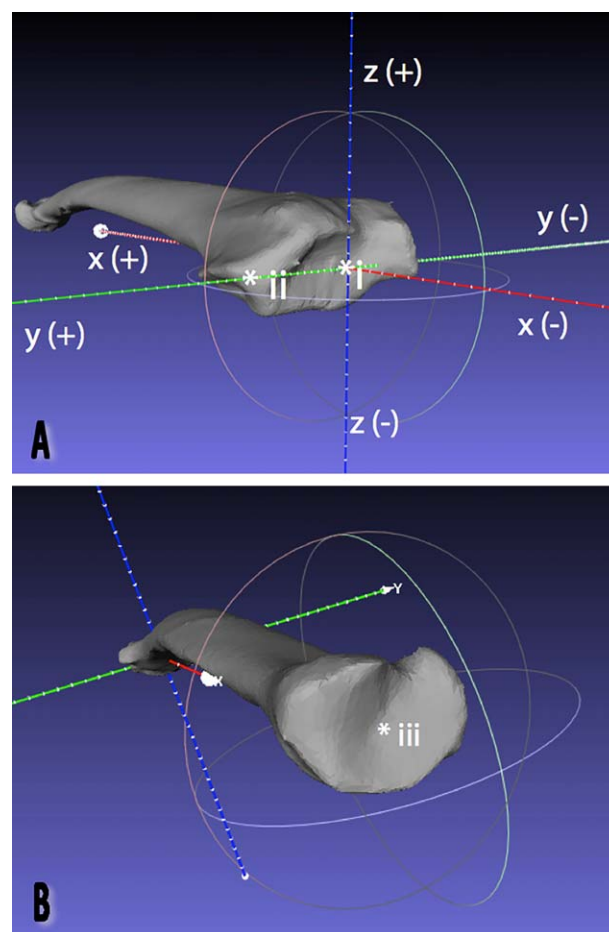
FIGURE 3 **A**, Alignment of the radius to the global (Cartesian) coordinate system, with the centrum of the distal radial articular surface (*) positioned at the origin of the coordinate system (*i) and the second axis orientation point at the craniodistal aspect of the ulnar notch (*ii). Note the labeled axes and their relative directional alignment (+ or −). **B**, The third coordinate orientation point was positioned at the centrum of the proximal radial articular surface (*iii)

Wolfram Research, Champaign, Illinois) was used to determine the rotation and translation matrix between 2 conditions of the extended position with or without ligament transection compared with the neutral position (Table 1). This was performed by using a Procrustes superimposition method to obtain the rotation and translation matrices.[14]

2.5 | Statistical analysis

Descriptive statistics were produced for carpal extension measurements. Statistical analysis was performed separately for each bone of the proximal carpal row. The rotation and translation matrices were decomposed into the rotation and translation values around (rotation) or along (translation) the global coordinate system x, y, and z axes. Each of the translation and rotation values in each axis for each of the condition comparisons was evaluated for normality by using a Shapiro-Wilk test, with $P > .05$ considered normally

TABLE 1 Testing conditions used to determine translation and rotation

Baseline condition	Comparison condition
Neutral (bilateral)	Extended (bilateral)
Neutral (group A)	Extended with PRL transection (group A)
Neutral (group B)	Extended with PUL transection (group B)
Neutral (group A)	Extended with PRL and PUL transection (group A)

PRL, palmar radiocarpal ligament; PUL, palmar ulnocarpal ligament.

distributed. Q-Q plots were reviewed for data that were not normally distributed according to Shapiro-Wilk test. Graphical statistics were used to describe the motions of the RCB, UCB, and ACB relative to the radius in limbs without ligament transection in neutral and extended positions. For the description of normal intact carpal kinematics, group A and group B limbs were grouped for the analysis.

For each of the individual bone analyses (RCB, UCB, ACB), a 1-way repeated-measures ANOVA was used to compare the 6 outcome variable (translation and rotation in 3 axes) differences of the intact limbs to each ligament transection condition. Sphericity was assessed by using Mauchly's test of sphericity with a Greenhouse-Geiser correction. This was performed for all repeated-measures ANOVA tests. $P > .05$ was used to establish sphericity. Bonferroni post hoc analyses were performed on each ANOVA condition comparison to assess for individual differences in means. A 1-tailed F-test was performed on the standard deviation data from each repeated-measures ANOVA to assess variance in rotation and translation data after each of the transection conditions. An F-value greater than a value corresponding to $P < .05$ was considered significant for unequal variances.

The loads recorded during each condition were evaluated for normality for the normal limbs and for each ligament transection condition. The Shapiro-Wilk test and Q-Q plots were evaluated for normality. The load applied to the limbs in each ligament transection condition were recorded and significant differences between load in these groups were evaluated with a one-way repeated measures ANOVA.

Two-tailed Pearson correlation analyses were used for load change between the neutral and extended position of each scan and the rotation and translation values, respectively. These correlations were performed for each axis and for each of the RCB, UCB, and ACB. The load change was calculated by subtracting the extended force measurement from the neutral force measurement. Each of the comparison conditions in Table 1 and the corresponding load change value were included for the correlation analysis. A correlation was considered significant at $P < .05$.

3 | RESULTS

All condition variable data were normally distributed according to Shapiro-Wilk testing and assessment of Q-Q Plots. Ten intact limbs and 5 each of PRL, PUL, and PRPU limbs were included for analysis. No limbs were excluded from the analysis. Mean ($\pm$SD) CT carpal angle was $12.44°$ ($\pm1.38°$) and $59.88°$ ($\pm1.66°$) for neutral and loaded scans, respectively.

3.1 | Normal antebrachiocarpal kinematic data

The mean rotations and translations between neutral and extended positions in the intact carpus are described graphically in Figures 4 and 5, visually in Figure 6, and numerically in Tables 2 and 3.
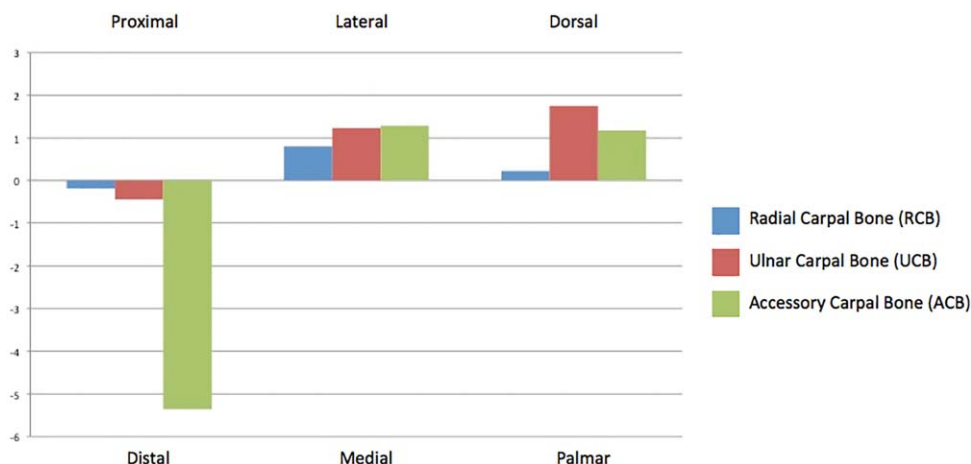
FIGURE 4 Mean translation (mm) of each bone of the proximal row of the intact carpus
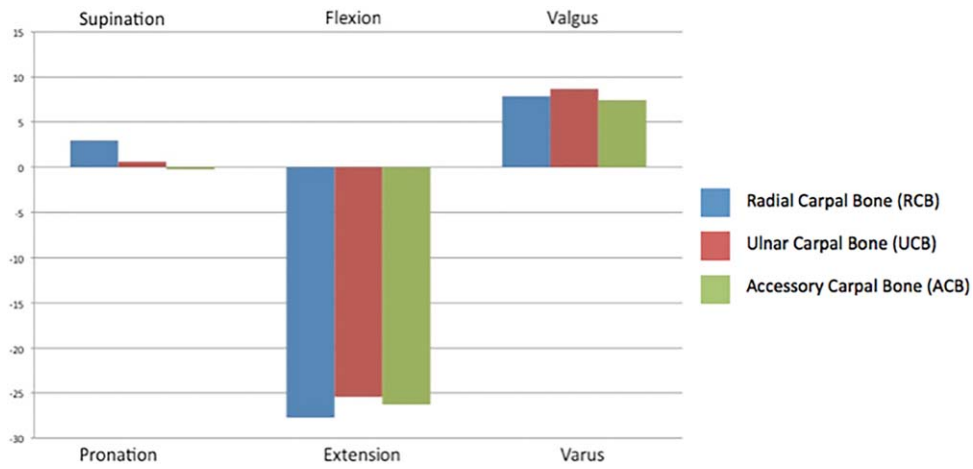
FIGURE 5 Mean rotation (degrees) of each bone of the proximal row of the intact carpus
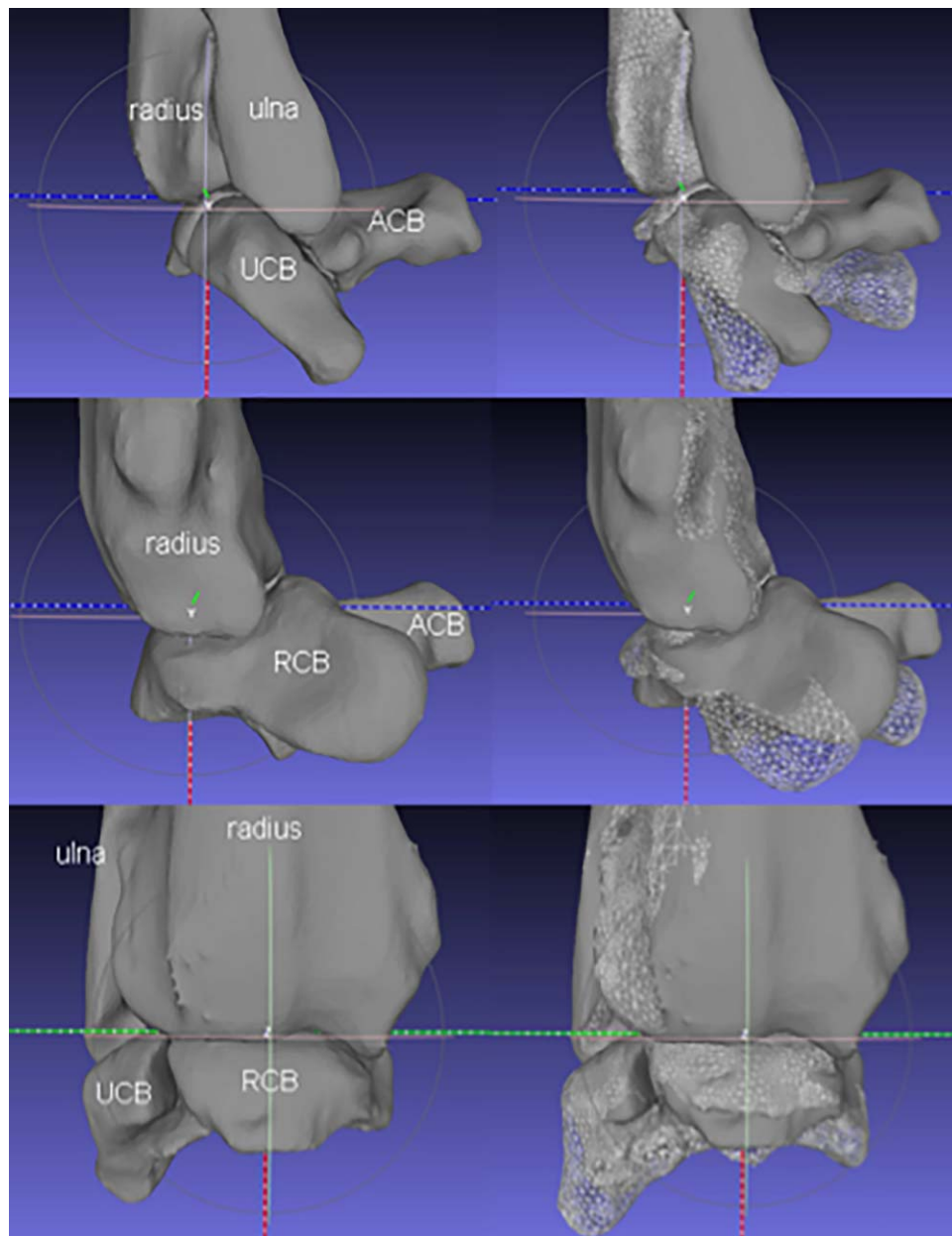
FIGURE 6 Lateral projection (top), medial projection (middle), and craniocaudal projection (bottom) of the antebrachiocarpal joint illustrating neutral position 3D model (solid gray bones, left) and extended position (wireframe gray bones, right)

TABLE 2 Translation of the RCB, UCB, and ACB along the x, y, and z axes after various ligament transections[a]

Bone	Axis	Condition				ANOVA results	
		Intact, no transection	PR transection	PU transection	PRPU transection	F value	P value
RCB	X	−0.19 (±0.63)	−0.17 (±0.50)	−0.18 (±0.72)	−0.27 (±0.80)	0.13	.94
	Y	0.80 (±0.31)	0.85 (±0.32)	0.60 (±0.26)	0.45 (±0.35)	1.23	.33
	Z	0.22 (±0.76)	0.29 (±0.59)	0.06 (±0.88)	0.13 (±1.47)	0.18	.91
UCB	X	−0.45 (±0.55)	−0.65 (±0.45)	−0.16 (±0.56)	−0.76 (±0.52)	1.62	.23
	Y	1.24 (±0.39)	1.24 (±0.41)	0.97 (±0.28)	1.17 (±0.51)	0.42	.75
	Z	1.75 (±0.52)	1.90 (±0.26)	1.37 (±0.42)	1.91 (±0.52)	1.44	.28
ACB	X	−5.36 (±1.07)	−5.58 (±0.90)	−4.88 (±1.08)	−5.98 (±1.43)	1.52	.26
	Y	1.28 (±0.65)	1.29 (±0.70)	1.06 (±0.24)	0.92 (±1.47)	0.17	.91
	Z	1.17 (±0.80)	1.31 (±0.62)	0.72 (±0.38)	1.48 (±1.03)	1.40	.29

ACB, accessory carpal bone; PR, palmar radiocarpal; PRPU, palmar radiocarpal and palmar ulnocarpal; PU, palmar ulnocarpal; RCB, intermedioradiocarpal bone; UCB, ulnar carpal bone.

[a]Positive translations along the x, y, and z axes represent proximal, lateral, and dorsal directions, respectively. Data are millimeters, mean (±SD).

3.2 | Transection of the palmar ligament

Sphericity was established in kinematic data of the neutral and extended position for each of the ligament transection conditions. When all 6 translation and rotation data groups were grouped and included in the repeated-measures ANOVA, rotation and translation values differed between the RCB (F = 142.81, $P < .001$), UCB (F = 115.90, $P < .001$), and ACB (F = 102.53, $P < .001$). Bonferroni post hoc analysis revealed no difference in translation (Table 2) or rotation (Table 3) between any of the compared ligament transection conditions (PRL, PUL, or PRL and PUL transection) in the RCB, UCB, or ACB in any axis.

Variance of the rotational data around the x-axis (pronation/supination) increased for all bones after PRL and PUL transection and for the UCB after PUL transection compared with the intact carpus group. In addition, variance of the rotation of the RCB around the y-axis (flexion/extension) increased (Table 4).

All loads applied to the limbs differed between neutral and extended positions (F = 68.508, $P < .001$). There was no difference in mean load applied to the limbs within the neutral

TABLE 3 Rotation of the RCB, UCB, and ACB around the x, y, and z axes after ligament transections[a]

Bone	Axis	Condition				ANOVA results	
		Intact, no transection	PR transection	PU transection	PRPU transection	F value	P value
RCB	x	2.95 (±2.18)	3.00 (±1.74)	2.40 (±1.96)	4.06 (±7.33)	0.22	.44
	y	−27.74 (±2.63)	−28.09 (±2.80)	−26.16 (±1.53)	−24.88 (±11.62)	0.37	.77
	z	7.89 (±4.99)	6.99 (±4.58)	8.18 (±5.07)	9.04 (±6.03)	0.18	.90
UCB	x	0.60 (±2.56)	0.88 (±1.80)	0.55 (±0.39)	1.56 (±6.27)	0.25	.86
	y	−25.43 (±2.7)	−25.52(±3.12)	−24.21 (±2.02)	−25.80 (±5.19)	1.53	.26
	z	8.70 (±4.53)	7.62 (±2.37)	9.00 (±3.91)	8.74 (±5.03)	0.15	.93
ACB	x	−0.25 (±2.63)	−1.26 (±2.88)	−1.07 (±1.39)	1.75 (±6.36)	0.92	.46
	y	−26.28 (±3.02)	−27.37 (±2.13)	−24.13 (±2.10)	−28.03 (±3.88)	3.07	.07
	z	7.46 (±4.92)	6.09 (±4.30)	8.09 (±5.22)	8.72 (±4.42)	0.34	.80

ACB, accessory carpal bone; PR, palmar radiocarpal; PRPU, palmar radiocarpal and palmar ulnocarpal; PU, palmar ulnocarpal; RCB, intermedioradiocarpal bone; UCB, ulnar carpal bone.

[a]Positive rotations around the x, y, and z axes represent pronation, flexion, and valgus, respectively. Data are degrees, mean (±SD).

TABLE 4 One-tailed F test describing variance in each outcome for each of the transection conditions compared with the intact condition[a]

Motion	Bone	Axis	PRL	PUL	PRPU
Translation, mm	RCB	X	1.59	1.31	1.61
		Y	0.94	0.70	1.27
		Z	1.66	1.34	3.74
	UCB	X	1.49	1.04	0.89
		Y	0.90	0.52	1.71
		Z	4.00	0.65	1.00
	ACB	X	1.41	1.02	1.79
		Y	0.86	0.14	5.11[b]
		Z	1.66	0.23	1.66
Rotation, °	RCB	X	1.57	1.24	11.31[b]
		Y	0.88	2.95	19.52[b]
		Z	1.19	0.97	1.46
	UCB	X	2.02	43.09[b]	6.00[b]
		Y	0.75	1.79	3.69
		Z	3.65	1.34	1.24
	ACB	X	0.83	3.58	5.85[b]
		Y	2.01	2.07	1.65
		Z	1.31	0.89	0.81

ACB, accessory carpal bone; PRL, palmar radiocarpal ligament; PRPU, palmar radiocarpal and palmar ulnocarpal; PUL, palmar ulnocarpal ligament; RCB, intermedioradiocarpal bone; UCB, ulnar carpal bone.
[a]$F > 5.05$, which corresponded to $P < .05$, was considered significant.
[b]Greater variance compared with intact.

or extended position groups when the intact normal condition was compared with each ligament transection condition ($F = 0.032$, $P = .995$ for neutral position; $F = 7.084$, $P = .274$ for extended position; Table 5).

3.3 | Correlations

No correlation was found between the kinematic data and the load change between carpal positions in the RCB, UCB, or ACB (Tables 6–7).

4 | DISCUSSION

Loading of the canine carpus induces extension but also a lesser degree of valgus and RCB supination. The antebrachiocarpal motion is therefore more complex than that of a pure ginglymus joint. We did not detect an influence of PRL

TABLE 5 Baseplate force measurements acquired by pressure sensitive film immediately prior to CT acquisition for each position and ligament transection condition

	Mean load ± SD (Newtons)	
Condition	Group A	Group B
Neutral intact	277.40 ± 200.01[a]	306.00 ± 130.34[a]
Extended intact	2148.20 ± 453.81[b]	2519.40 ± 277.70[b]
Neutral PRL transection	314.80 ± 148.43[a]	. . .
Extended PRL transection	2110.80 ± 565.77[b]	. . .
Neutral PRPU transection	301.00 ± 140.46[a]	. . .
Extended PRPU transection	1959.00 ± 456.50[b]	. . .
Neutral PUL transection	. . .	300.60 ± 165.29[a]
Extended PUL transection	. . .	2340.80 ± 426.68[b]

. . ., no data; CT, computed tomography; PRL, palmar radiocarpal ligament; PRPU, palmar radiocarpal and palmar ulnocarpal ligament; PUL, palmar ulnocarpal ligament.
[a]Not significantly different loads recorded in neutral limbs.
[b]Not significantly different loads recorded in extended limbs.

or PUL transection on mean carpal bone translation or rotation or on limb load. However, combined PRL and PUL transection and, to a lesser degree, PUL transection increased variance of the kinematic data in transverse and sagittal planes.

The relative rotation of each of the bones around the y-axis (25.43°-27.74°) can be explained by the major contribution of the antebrachiocarpal joint to overall carpal extension. Although additional studies are required to determine the relative contributions of each joint level to carpal extension, this study highlights the possible misunderstanding, based on the current literature, of canine carpal motion. Carpal extension varied by 48° between neutral and loaded positions in this study. The extension of the RCB was 27.74°, which would account for 58% of the total carpal extension and is less than previously postulated. Instead, the middle carpal

TABLE 6 Pearson correlation of load change between neutral and extended carpal positions and translations of the RCB, UCB, and ACB in all axes

	RCB		UCB		ACB	
Axis	R²	P value	R²	P value	R²	P value
x	−0.10	0.63	−0.09	0.69	0.20	0.36
y	0.09	0.66	−0.10	0.64	−0.23	0.27
z	0.13	0.54	−0.01	0.59	−0.36	0.07

ACB, accessory carpal bone; RCB, intermedioradiocarpal bone; UCB, ulnar carpal bone.

TABLE 7 Pearson correlation of load change between neutral and extended carpal positions and rotations of the RCB, UCB, and ACB in all axes

Axis	RCB		UCB		ACB	
	R^2	*P* value	R^2	*P* value	R^2	*P* value
x	0.019	0.93	−0.11	0.61	0.19	0.37
y	−0.13	0.54	0.23	0.27	0.29	0.16
z	−0.10	0.64	−0.11	0.60	0.06	0.78

ACB, accessory carpal bone; RCB, intermedioradiocarpal bone; UCB, ulnar carpal bone.

and carpometacarpal joints seemed to contribute considerably to carpal extension when subjected to the highest physiologic loads required to achieve the carpal extension tested in the present study.[15,16] The carpus was tested here in 2 static positions, and each carpal joint may contribute differently to overall joint motion at varying magnitudes of loading. A recent study of human carpal bones found a negligible difference in the joint axes and movements for carpal bones, as calculated from either a real time "4-dimensional" dynamic system or a stepwise method of interpolation between bone positions in different wrist postures.[17] Hence, the method used in the present study provides accurate positional data in the context of highly consistent motion in the intact carpus. This consistency of kinematic data in the intact limbs on the basis of pilot studies determined the selection of the sample size used for this study.

The antebrachiocarpal motion measured in intact limbs was a ginglymus in the sagittal plane but also included smaller but consistent rotations of the RCB, UCB, and ACB around the z-axis of the radius (valgus) and of the RCB around the x-axis (supination). The mean valgus rotation of the RCB, UCB, and ACB ranged between 7.45° and 8.70° around the z-axis. In addition, the RCB pronated a mean of 2.95° during loading of the carpus, whereas this rotation was not as evident in the UCB or the ACB. From these findings, we can reject our first hypothesis that, under axial load, intact greyhound carpal kinematics involve translations and rotations limited to a pure sagittal plane ginglymus. Although this study described a considerably greater distal translation of the ACB compared with the RCB and UCB, this measurement was influenced by the eccentricity of the ACB to the x-axis, creating a larger arc through which it rotated. When this factor is taken into consideration, the predominant mode of motion of the bones at the antebrachiocarpal joint (Tables 2–3) consists of rotation, with a required translation or a combined (helical screw) mode.

The role of the palmar antebrachiocarpal stabilizers, as it has been discussed in the current literature, remains unclear. One study reported alterations in carpal extension after transection of both the palmar antebrachiocarpal ligaments, with similar effects produced by medial and lateral collateral ligament transection.[7] Another subjective report proposed a predominant role of the PUL in limiting dorsal and palmar drawer of the manus.[8] Our second hypothesis, that transection of the PRL and/or the PUL would not influence carpal bone motion or limb load, was based on the absence of studies investigating axially loaded canine carpi to defined displacements rather than to defined loads as well as varied reports of PRL and PUL function with other types of testing. Limb load or mean position of the carpal bones was not influenced by ligament transections in our study, suggesting a less important role of these structures in limiting extension. Although mean translation or rotation data did not change after PRL, PUL, or combined PRL and PUL transections, the variance of rotations increased. This change occurred mainly around the x-axis for all bones and around the y-axis for the RCB after combined PRL and PUL transection (Tables 3–4). These results provide evidence for an increased variation in rotation of these bones in the transverse (pronation/supination) plane and, to a lesser extent, the sagittal (flexion/extension) plane, especially after combined ligament transection (Table 4). Increased rotational variance was noted only once in the x-axis for the UCB, after single PUL transection, and this increase was also evident after combined ligament transection for this bone and plane. Because the variability of intact limb rotational motion in the transverse and sagittal planes is consistently minimal, these findings provide evidence for a possible role of the PRL and the PUL in stabilization of the antebrachiocarpal joint in multiple planes during carpal loading. Alterations in variance does not justify rejection of the second hypothesis; transection of the PRL or the PUL did not significantly affect antebrachiocarpal motion compared with control carpal joints because ligament transection did not change mean kinematic data.

Specimens in this study were investigated at 2 angular displacements. Specimen testing at different extension angles may provide additional information about the role of the PRL and the PUL. Specifically, at lower extension angles, the PRL and/or the PUL may theoretically function to partially limit extension, whereas, at the higher extension angle tested in the present study, a more important function may be limiting carpal bone instability in multiple planes (pronation/supination and flexion/extension), as we have demonstrated.[7] Inclusion of additional antebrachiocarpal stabilizer transection conditions (palmar flexor retinaculum, medial and lateral collateral ligaments, accessorometacarpal ligaments) may also be used with the techniques described in this study to evaluate the comparative role of the PRL and the PUL.

Assessing the carpus at predetermined angular displacements was selected over a model using a standardized load to minimize large differences in carpal extension angle as a

confounding variable. The wide standard deviation in grouped load measurements for each ligament transection condition indicate interspecimen variation in load. As such, this measurement was used to determine whether ligament transection was associated with an effect on load.[7,18] The viscoelastic phenomenon of mechanical creep was evident when forces imparted by the limb to the baseplate of the jig were measured, in that these forces gradually but continuously decreased during the time that the limbs were maintained in position. This was most evident prior to preconditioning the limbs. The number of preconditioning cycles performed on each limb was selected on the basis of previous studies demonstrating the steady state of mechanical creep achieved after 10 cycles.[19,20] The carpal angle in the 60° position was selected on the basis of observation of greyhounds during the initial forelimb stance of a "double-suspension rotary gallop." Extension angles exceeding 60° have also recently been reported in an in vivo study of agility dogs entering the A-Frame.[3] We do not believe that specimens underwent substantial plastic deformation during testing due to there being no significant difference in neutral or extended limb load between ligament transection conditions.

The use of cadaveric specimens in this study precluded evaluation of the active stabilizers of the carpus. Kinematic analysis of the antebrachiocarpal joint in only 2 carpal positions was also a limitation, although interpolation between the 2 positions has previously been found to describe accurately data obtained from dynamic methods.[17] A series of positions may be selected in future studies to evaluate changes in intermediate stages and other planes of motion. In addition, the limited number of specimens tested may have masked small mean kinematic differences between transection groups.

This study describes a kinematic methodology that can be applied to other joints, breeds, or species for assessment of internal joint motion. A description of the contribution of each of the middle carpal and carpometacarpal joints to overall carpal motion may be one such example. Development of these kinematic data for the canine carpus with description of functional units of the joint may lead to novel surgical techniques to treat canine carpal pathologies.[21]

CONFLICT OF INTEREST

ORCID

Jack D. Neville-Towle BVSc http://orcid.org/0000-0002-9152-8462

REFERENCES

[1] Yalden DW. The functional morphology of the carpal bones in carnivores. *Acta Anatomica*. 1970;77:481-500.

[2] Holler P, Brazda V, Dal-Bianco B, et al. Kinematic motion analysis of the joints of the forelimbs and hind limbs of dogs during walking exercise regimens. *Am J Vet Res*. 2010;71:734-741.

[3] Appelgrein C, Glyde M, Hosgood G, et al. Measurement of carpal joint extension in agility dogs entering the A-Frame, *Vet Surg*. 2017;46;E20 (abstract).

[4] Crisco JJ, McGovern RD, Wolfe SW. Noninvasive technique for measuring in vivo three-dimensional carpal bone kinematics. *J Orthop Res*. 1999;17:96-100.

[5] Rainbow M, Kamal R, Leventhal E, et al. In vivo kinematics of the scaphoid, lunate, capitate, and third metacarpal in extreme wrist flexion and extension. *J Hand Surg*. 2013;38A:278-288.

[6] Mikic Z, Ercegan G, Somer T. Detailed anatomy of the antebrachiocarpal joint in dogs. *Anat Rec*. 1992;233:329-334.

[7] Milgram J, Milshtein T, Meiner Y. The role of the antebrachiocarpal ligaments in the prevention of hyperextension of the antebrachiocarpal joint. *Vet Surg*. 2012;41:191-199.

[8] Warnock J, Beale B. Arthroscopy of the antebrachiocarpal joint in dogs. *J Am Vet Med Assoc*. 2004;224:867-874.

[9] Gregersen C, Silverton N, Carrier D. External work and potential for elastic storage at the limb joints of running dogs. *J Exp Biol*. 1998;201:3197-3210.

[10] Williams S, Daynes J, Peckham K, et al. Functional anatomy and muscle moment arms of the thoracic limb of an elite sprinting athlete: the racing greyhound (*Canis familiaris*). *J Anat*. 2008;213:373-382.

[11] Tan C, Parr W, Walsh W, et al. Influence of scan resolution, thresholding and smoothing on computed tomography (CT) based kinematic measurements. *J Biomech Eng*. 2017;139: 1045031-1045035.

[12] Cignoni P, Callieri M, Corsini M, et al. MeshLab: an open-source mesh processing tool. In: Sixth Eurographics Italian Chapter Conference Proceedings; July 2-4, 2008; Salerno, Italy. p 129-136.

[13] Besl PJ, McKay ND. A method for registration of 3-D shapes. *IEEE Trans Pattern Anal Mach Intell*. 1992;14:239-256.

[14] Gower JC. Generalized Procrustes analysis. *Psychometrika*. 1975;40:33-51.

[15] Yanoff S, Hulse D, Hogan H, et al. Measurements of vertical ground reaction force in jumping dogs. *Vet Comp Orthop Traumatol*. 1992;5:44-50.

[16] Hudson P, Corr S, Wilson A. High speed galloping cheetah (*Acinonyx jubatus*) and the racing greyhound (*Canis familiaris*): spatiotemporal and kinetic characteristics. *J Exp Biol*. 2012;215: 2425-2434.

[17] Foumani M, Strackee SD, Jonges R, et al. In vivo three-dimensional carpal bone kinematics during flexion-extension and radio-ulnar deviation of the wrist: dynamic motion versus stepwise static wrist positions. *J Biomech*. 2009;42:2664-2671.

[18] Shetye S, Malhotra K, Ryan S, et al. Determination of mechanical properties of canine carpal ligaments. *Am J Vet Res*. 2009; 70:1026-1030.

[19] Yamamoto E, Hayashi K, Yamamoto N. Mechanical properties of collagen fascicles from stress-shielded patellar tendons in the rabbit. *Clin Biomech (Bristol, Avon)*. 1999;14(6):418-425.

[20] Woo S. Mechanical properties of tendons and ligaments. I. Quasi-static and nonlinear viscoelastic properties. *Biorheology*. 1982;19:385-396.

[21] Wolf P, Stacoff A, Liu A, et al. Functional units of the human foot. *Gait Posture*. 2008;28:434-441.